BSTR, 2023, Vol 11, No 1, 33-43
https://doi.org/10.54987/bstr.v11i1.834

HIBISCUS PUBLISHER

BIOREMEDIATION SCIENCE AND TECHNOLOGY RESEARCH

Website: http://journal.hibiscuspublisher.com/index.php/BSTR/index

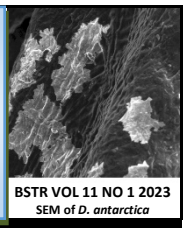

Isothermal Remodelling of the Biosorption of Congo Red onto Kaolin

Faggo Abdullahi Adamu[1,2], Ain Aqilah Basirun[1], Ahmad Syazwan Ismail[1], Mohd Ezuan Khayat[1] and Mohd Yunus Shukor[1]*

[1]Department of Biochemistry, Faculty of Biotechnology and Biomolecular Sciences, Universiti Putra Malaysia, 43400 UPM Serdang, Selangor, Malaysia.
[2]Department of Microbiology, Faculty of Science, Bauchi State University Gadau, Bauchi, PMB 065, Nigeria.

*Corresponding author:
Mohd Yunus Shukor,
Department of Biochemistry,
Faculty of Biotechnology and Biomolecular Sciences,
Universiti Putra Malaysia,
43400 UPM Serdang,
Selangor,
Malaysia.
Email: mohdyunus@upm.edu.my

HISTORY

Received: 12th April 2023
Received in revised form: 24th June 2023
Accepted: 28th June 2023

KEYWORDS

Congo Red
Adsorption
Kaolinite
Freundlich
Langmuir

ABSTRACT

A remodeling analysis was conducted on the sorption isotherm data for Congo Red adsorption onto kaolin using nonlinear regression. (CR) also known as 1-naphthalenesulfonic acid, 3,3′-(4,4′-biphenylenebis(azo)) bis(4-amino-) disodium salt, is a synthetic anionic azo dye widely utilized in various industrial sectors, including rubber, plastic, textiles, paper, and printing. This dye is of significant interest due to its versatile applications and unique chemical properties. To prevent overfitting due to the limited data points, isotherm models with up to three parameters were utilized. Statistical analysis based on error function assessments, including root-mean-square error (RMSE), adjusted coefficient of determination (adjR^2), accuracy factor (AF), bias factor (BF), Bayesian Information Criterion (BIC), corrected AICc (Akaike Information Criterion), and Hannan-Quinn Criterion (HQC), revealed that the best performance was achieved by the Freundlich model, followed by the Langmuir and Jovanovic models, which ranked as the top three models.The best isotherm model was found to be the Unilan followed by (descending order) Brouers–Sotolongo, Hill, Sips and Langmuir. The Unilan maximum adsorption capacity, shows large deviation from the experimentally observed value with a large 95% confidence interval, indicating poor fitting parameters despite being the best model based on the error function analysis. The next best model was Brouers–Sotolongo with a maximum adsorption capacity, q_{mBS} of 5.48 mg g^{-1} (95% confidence interval from 4.791 to 6.172) which agrees with experimental observations. The value of the maximum monolayer adsorption capacity for Congo Red binding to kaolin according to the Langmuir's parameter q_{mL} was 5.49 mg g^{-1} (95% Confidence interval from 5.018 to 5.967), while b_L (L mg^{-1}), the Langmuir model constants was 0.5 L mg^{-1} (95% C.I. from 0.285 to 0.710).

INTRODUCTION

The world is facing a great challenge in ensuring widespread access to clean and safe drinking water. Water pollution occurs when environmental stressors are introduced at concentrations exceeding the maximum permissible levels, rendering water unsuitable for consumption and various other purposes. Such pollution stems from the presence of organic and/or inorganic chemicals, minerals, or waste materials originating from diverse sources, including industrial, agricultural, clinical, and domestic activities [1–5]. Of these sources, industrial effluents emerge as the most significant contributors to the contamination of surface and groundwater. This phenomenon is exacerbated by the rapid process of globalization and urbanization, which fuels the demand for products manufactured using dyes and heavy metals [6–11]. Notably, heavy metals like copper (Cu) and lead (Pb) are commonly found in the wastewater of industries situated in smelting, electrical, and mining areas[12–14]. Meanwhile, dyes and pigments are prevalent in the effluents of sectors such as food, textiles, and pharmaceuticals, where these substances are employed as colorants. It is crucial to highlight the carcinogenic and mutagenic properties of these non-biodegradable and highly toxic chemicals [15–19].

Dyes, broadly categorized into various types, are essential in industries like textiles, with approximately 8×10^5 tons of synthetic dyes produced annually [15,20,21]. The textile sector alone accounts for roughly 75% of the global dyestuff market, employing a wide array of dyes for fabric coloring and printing . However, excessive dye usage can lead to poor fixation on

materials, causing surface water and groundwater contamination through effluent discharge, visible as undesirable color, and negatively impacting aquatic ecosystems. Dye pollution diminishes light penetration, elevates biochemical oxygen demand (BOD), and impairs photosynthetic activities in aquatic flora, affecting the food sources of aquatic organisms [22–26]. Beyond ecological concerns, synthetic dye discharge renders water aesthetically unpleasant and raises health worries, as studies have identified genotoxic, mutagenic, and carcinogenic effects from the consumption of water containing synthetic dyes [27–29]. Congo Red (CR) possesses a stable aromatic structure, rendering it non-biodegradable and harmful to both aquatic organisms and human health [17,30–33]. Consequently, it becomes imperative to address effluents containing CR before their discharge into the environment. Extensive research by scientists has yielded a plethora of treatment technologies for CR, encompassing physical, chemical, and biological approaches, each accompanied by its distinct set of challenges, drawbacks, advantages, limitations, applicability, and cost considerations.

Adsorption serves as a highly effective and safe method for purifying contaminated water, offering cost-efficiency without associated hazards. Adsorbents utilized in this process can be derived from various sources, including microbial biomass, inorganic substances, and natural substrates [8,34–37]. Recent years have witnessed substantial research into the biosorption of mercury, yielding high-quality results achieved at a reasonable cost. Low-cost adsorbents play a crucial role in this context, encompassing materials readily available in large quantities, abundant in nature, or generated as by-products in industrial processes. One of the primary applications of kaolin lies in its use as a versatile material in various industries. Kaolin finds significant utility in drilling mud, where it serves as a critical component. Additionally, it functions as a binder, purifier, absorbent, and carrier for fertilizers or pesticides. Notably, around 1990, nearly half of the United States' kaolin production was dedicated to its use in drilling mud, underlining its importance in this sector. Kaolin also finds applications as a filler, sealant, and catalyst in petroleum refining processes, further showcasing its versatility and utility across different industries [38–40].

A precise analysis of the kinetics and isotherms in the biosorption process is essential for gaining a comprehensive understanding of this phenomenon in various species. Scientific literature often presents linearized representations of what are inherently nonlinear curves in such data. However, the process of linearizing inherently nonlinear data alters the error structure associated with it. A drawback of this approach is that it tends to invalidate the assumption of a Gaussian distribution of residuals for the transformed data [41]. Consequently, quantifying uncertainty becomes more challenging, often depicted as a 95 percent confidence range. This study aims to revisit and reanalyze a previously published work on Congo Red sorption onto kaolin [42], which employed linear regression to derive the best-fitting models.

METHODs

Data acquisition and fitting

Figure 6a data from a previously published study [42] was digitized using the freeware Webplotdigitizer 2.5 [43]. Digitization using this program has been praised for its dependability [44]. After that, the data were nonlinearly regressed using the curve-fitting program Curve-Expert Professional (Version 2.6.5, copyright Daniel Hyams). Implicit equations were solved using MATLAB (Mathworks, Massachusetts, United States).

Isotherms

As the value of the data points is very small, only models having parameters of up to three were considered to prevent overfitting.

Table 1. Mathematical models that were used in modelling data [45,46].

Isotherm	p	Formula	Ref.
Henry's law	1	$q_e = HC_e$	[47]
Langmuir	2	$q_e = \frac{q_{mL} b_L C_e}{1 + b_L C_e}$	[45]
Jovanovic	2	$q_e = q_{mJ}(1 - e^{-K_J C_e})$	[48]
Freundlich	2	$q_e = K_F C_e^{\frac{1}{n_F}}$	[49]
Dubinin-Radushkevich	2	$q_e = q_{mDR} exp\left\{-K_{DR}\left[RTln\left(1+\frac{1}{C_e}\right)\right]^2\right\}$	[50,51]
Temkin	3	$q_e = \frac{RT}{b_T}\{ln(a_T C_e)\}$	[52,53]
Redlich-Peterson	3	$q_e = \frac{K_{RP1} C_e}{1 + K_{RP2} C_e^{\beta_{RP}}}$	[54]
Sips	3	$q_e = \frac{K_s q_{mS} C_e^{\frac{1}{n_S}}}{1 + K_s C_e^{\frac{1}{n_S}}}$	[55]
Toth	3	$q_e = \frac{q_{mT} C_e}{\left(K_T + C_e^{n_T}\right)^{\frac{1}{n_T}}}$	[56]
Hill	3	$q_e = \frac{q_{mH} C_e^{n_H}}{K_H + C_e^{n_H}}$	[57]
Khan	3	$q_e = \frac{q_{mK} b_K C_e}{(1 + b_K C_e)^{a_K}}$	[58]
BET	3	$q_e = \frac{q_{mBET} \alpha_{BET} C_e}{(1 - \beta_{BET} C_e)(1 - \beta_{BET} C_e + \alpha_{BET} C_e)}$	[59]
Vieth-Sladek	3	$q_e = \frac{q_{mVS} b_{VS} C_e}{(1 + b_{VS} C_e)^{n_{VS}}}$	[60]
Radke-Prausnitz	3	$q_e = \frac{A_{RP} B_{RP} C_e^{\beta}}{A_{RP} + B_{RP} C_e^{\beta - 1}}$	[61–63]
Brouers–Sotolongo	3	$q_e = q_{mBS}\left(1 - \exp\left(-K_{BS} C_e^{\frac{1}{n_{BS}}}\right)\right)$	[64,65]
Fritz-Schlunder-III	3	$q_e = \frac{q_{mFS} K_{FS} C_e}{1 + K_{FS} C_e^{n_{FS}}}$	[66]
Fowler-Guggenheim*	3	$q_e = q_{mFG} \frac{K_L C_e e^{\frac{\alpha q_e}{q_{mFG}}}}{1 + K_L C_e e^{\frac{\alpha q_e}{q_{mFG}}}}$	[67]
Moreau	3	$q_e = q_{mM} \frac{bC_e + lb^2 C_e^{\,2}}{1 + 2bC_e + lb^2 C_e^{\,2}}$	[68]
Unilan	3	$q_e = \frac{q_{mU}}{2b_U} ln\left(\frac{a_U + C_e e^{b_U}}{a_U + C_e e^{-b_U}}\right)$	
Baudu	4	$q_e = \frac{q_{mB} b_B C_e^{(1+x+y)}}{1 + b_B C_e^{(1+x)}}$	[69]
Marczewski-Jaroniec	4	$q_e = q_{mMJ}\left(\frac{(K_{MJ} C_e)^{n_{MJ}}}{1 + (K_{MJ} C_e)^{n_{MJ}}}\right)^{\frac{m_{MJ}}{n_{MJ}}}$	[70]
Fritz-Schlunder-IV	4	$q_e = \frac{A_{FS} C_e^{a_{FS}}}{1 + B_{FS} C_e^{b_{FS}}}$	[66]
Weber-van Vliet*	4	$C_e = P_1 q_e^{\left(P_2 q_e^{P_3} + P_4\right)}$	[71]

Note *Implicit equation or function.

Statistical analysis

A set of statistical discriminatory tests such as corrected AICc (Akaike Information Criterion), Bayesian Information Criterion (BIC), Hannan and Quinn's Criterion (HQ), Root-Mean-Square Error (RMSE), bias factor (BF), accuracy factor (AF) and adjusted coefficient of determination (R^2) were used in this study.

The RMSE was computed using Equation 1, and it stands to reason that the fewer parameters utilized, the smaller the RMSE will be. n is for the total number of observations made in the experiment, Obi and Pdi stand for the total number of observations made in the experiment and projections, and p stands for the total number of parameters [41] .

$$RMSE = \sqrt{\frac{\sum_{i=1}^{n}(Pd_i - Ob_i)^2}{n-p}} \qquad \text{(Eqn. 1)}$$

Because R^2 or the coefficient of determination ignores the number of parameters in a model, the modified R^2 is used to overcome this limitation. The entire variance of the y-variable is given by S^2_y in the equation (**Equations 2** and **3**), while RMS is the Residual Mean Square.

$$Bias\ factor = 10\left(\sum_{i=1}^{n} log\frac{(Pd_i/Ob_i)}{n}\right) \qquad \text{(Eqn. 2)}$$

$$Accuracy\ factor = 10\left(\sum_{i=1}^{n} log\frac{|(Pd_i/Ob_i)|}{n}\right) \qquad \text{(Eqn. 3)}$$

The AICc is computed as follows (**Equation 4**), where p represents the number of parameters and n represents the number of data points. The corrected Akaike information criterion (AICc) is used to manage data with a large number of parameters but a limited number of values [72]. A model with a lower AICc score is considered more likely to be right [72]. The information theory is the foundation of the Akaike Information Criterion (AIC). It strikes a compromise between the goodness of fit of a given model and the model's complexity [73].

$$AICc = 2p + n\ln\left(\frac{RSS}{n}\right) + \frac{2(p+1)+2(p+2)}{n-p-2} \qquad \text{(Eqn. 4)}$$

Another statistical tool based on information theory apart from AICc, is the Bayesian Information Criterion (BIC) (Equation 5). The number of parameters is penalized more severely by this error function than by AIC [74].

$$BIC = n\ln\left(\frac{RSS}{n}\right) + k\ln(n) \qquad \text{(Eqn. 5)}$$

The Hannan-Quinn information criterion (HQC) (**Equation 6**) is another error function approach based on information theory. Because of the ln ln n element in the calculation, the HQC is more consistent than the AIC [72].

$$HQC = nIn\left(\frac{RSS}{n}\right) + 2k\ln(\ln n) \qquad \text{(Eqn. 6)}$$

The Accuracy Factor (AF) and Bias Factor (BF) are two further error function analyses derived from Ross's work [72]. These error functions evaluate models statistically for goodness-of-fit but do not penalize for the number of parameters (**Equations 7** and **8**).

$$Adjusted\ (R^2) = 1 - \frac{RMS}{S_Y^2} \qquad \text{(Eqn. 7)}$$

$$Adjusted\ (R^2) = 1 - \frac{(1-R^2)(n-1)}{(n-p-1)} \qquad \text{(Eqn. 8)}$$

Marquardt's percent standard deviation (MPSD) is another penalty-imposed error function that has been extensively utilized in numerous isotherm studies. The function has some similarity to a geometric mean error distribution that is altered according to the system's number of degrees of freedom [75]. Among the first to use this error function in the adsorption field is [76] and the error function's official term that is known as MPSD (Equation 9) was introduced by the McKay group [77].

$$MPSD = 100\sqrt{\frac{1}{n-p}\sum_{i=1}^{n}\left(\frac{Ob_i - Pd_i}{Ob_i}\right)^2} \qquad \text{(Eqn. 9)}$$

where n is the number of experimental data, p is the number of parameters, Ob_i is the experimental data, and Pd_i is the value predicted by the model.

RESULTS AND DISCUSSION

The equilibrium data presented in (Homagai et al., 2022) underwent analysis using various models, including Moreau, BET, Vieth-Sladek, Khan, Radke-Prausnitz, Toth, Freundlich, Fritz-Schlunder III, Hill, Sips, Brouers–Sotolongo, Temkin, Unilan, Langmuir, Jovanovic, Fowler-Guggenheim, Redlich-Peterson, Henry, and Dubinin-Radushkevich, which were employed for optimal fitting through non-linear regression. Notably, all of these models exhibited favorable fits with the data, except for the Henry and Dubinin-Radushkevich models, as illustrated in **Figures 1 to 19.**

The Unilan isotherm model was identified as the best-performing model based on a combination of evaluation criteria, including the smallest RMSE, high adjusted R^2, Bayesian Factor (BF), and AICc values approaching unity. However, when considering AICc as the error function, the Langmuir model ranked first. In the majority error function analysis, using Unilan as an example, the subsequent best-performing models in descending order were Brouers–Sotolongo, Hill, Sips, and Langmuir. Despite Unilan's top ranking, its maximum adsorption capacity exhibited significant deviation from experimental values, with a large 95% confidence interval, suggesting a poor fit. In contrast, the Brouers–Sotolongo model demonstrated a more accurate maximum adsorption capacity estimation (qm_{BS}) of 5.48 mg g^{-1}, with a 95% confidence interval of 4.791 to 6.172, aligning better with experimental observations. As enough models fitted well with the kaolin data, it explains and justifies the accuracy of using nonlinear regression as against the linear regression used in the original publication which only reported the use of the linearised forms of the Langmuir and the Freundlich models.

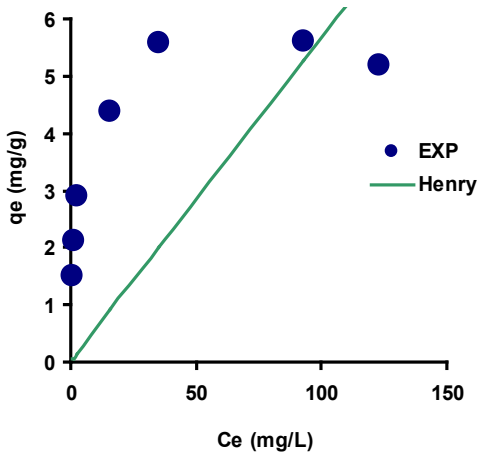

Fig. 1. Congo Red's adsorption isotherm onto kaolin as modelled using the Henry model.

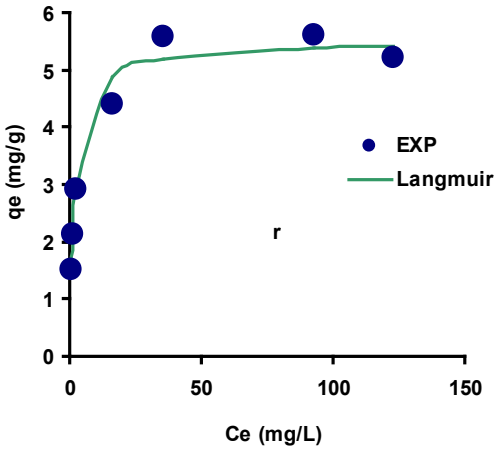

Fig. 2. Congo Red's adsorption isotherm onto kaolin as modelled using the Langmuir isotherm model.

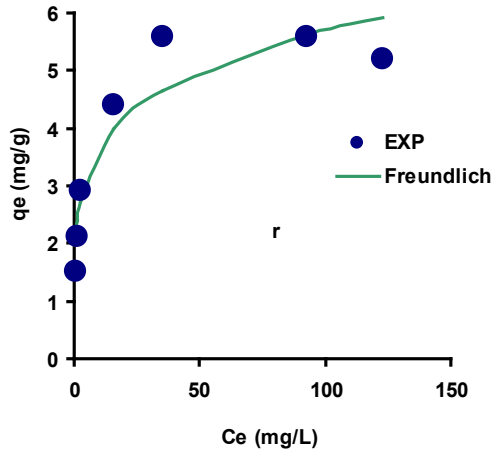

Fig. 3. Congo Red's adsorption isotherm onto kaolin as modelled using the Freundlich isotherm model.

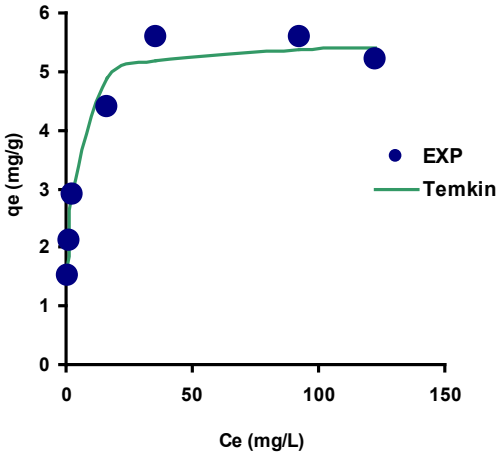

Fig. 4. Congo Red's adsorption isotherm onto kaolin as modelled using the Temkin isotherm model.

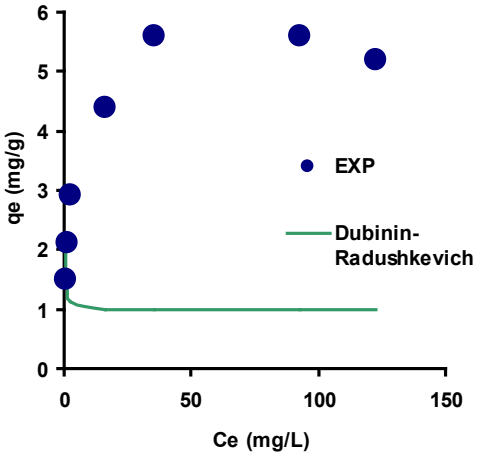

Fig. 5. Congo Red's adsorption isotherm onto kaolin as modelled using the Dubinin-Radushkevich isotherm model.

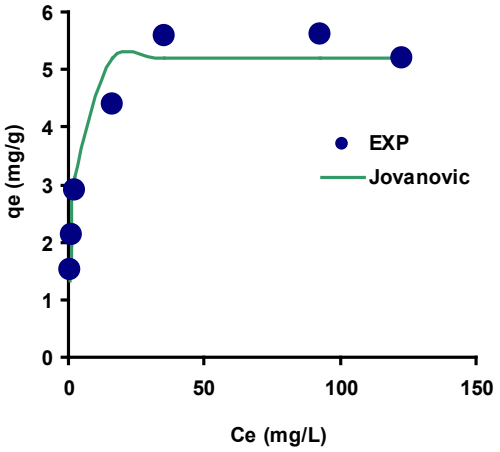

Fig. 6. Congo Red's adsorption isotherm onto kaolin as modelled using the Jovanovic isotherm model.

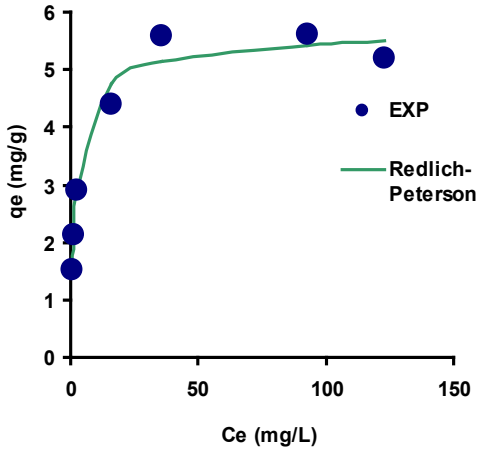

Fig. 7. Congo Red's adsorption isotherm onto kaolin as modelled using the Redlich-Peterson isotherm model.

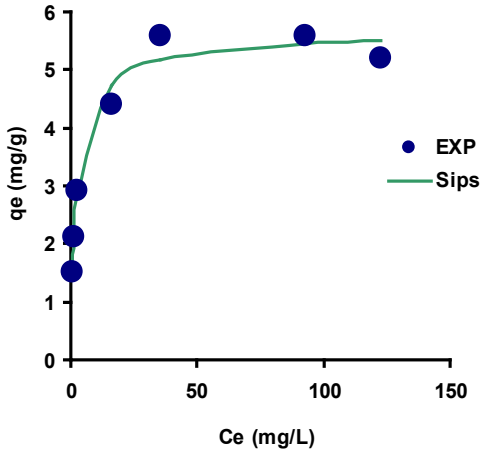

Fig. 8. Congo Red's adsorption isotherm onto kaolin as modelled using the Sips isotherm model.

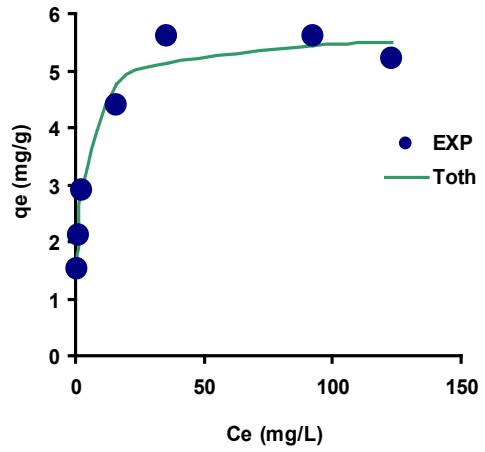

Fig. 9. Congo Red's adsorption isotherm onto kaolin as modelled using the Toth isotherm model.

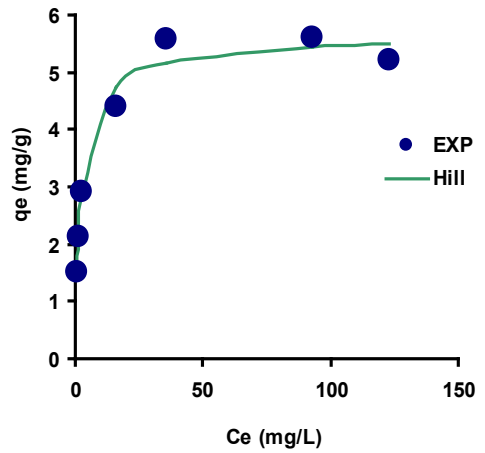

Fig. 10. Congo Red's adsorption isotherm onto kaolin as modelled using the Hill isotherm model.

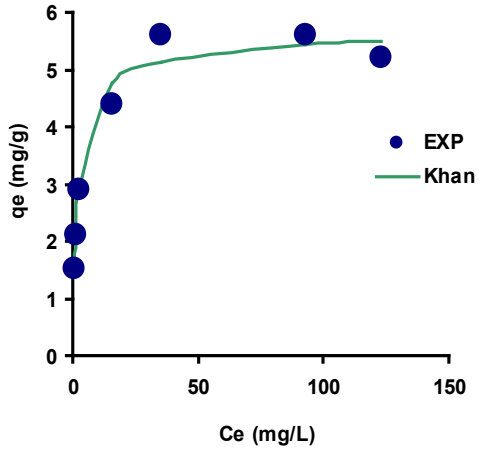

Fig. 11. Congo Red's adsorption isotherm onto kaolin as modelled using the Khan isotherm model.

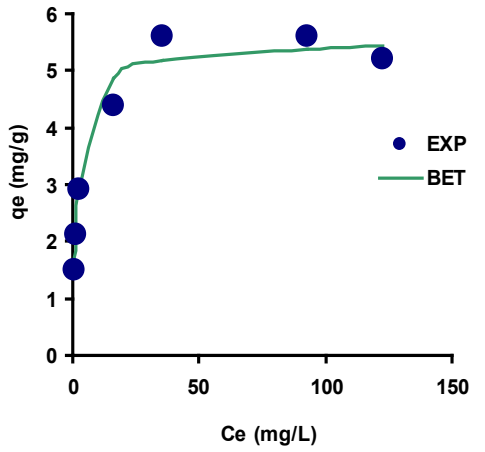

Fig. 12. Congo Red's adsorption isotherm onto kaolin as modelled using the BET isotherm model.

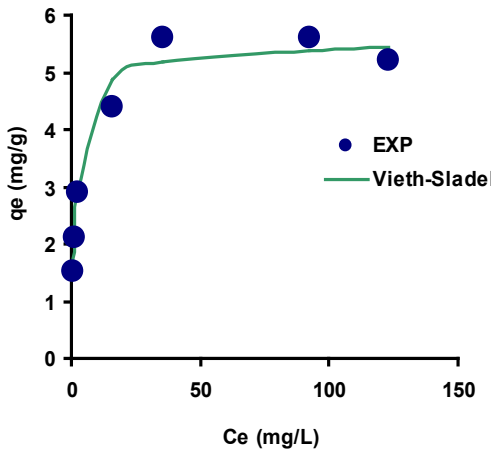

Fig. 13. Congo Red's adsorption isotherm onto kaolin as modelled using the Vieth-Sladek isotherm model.

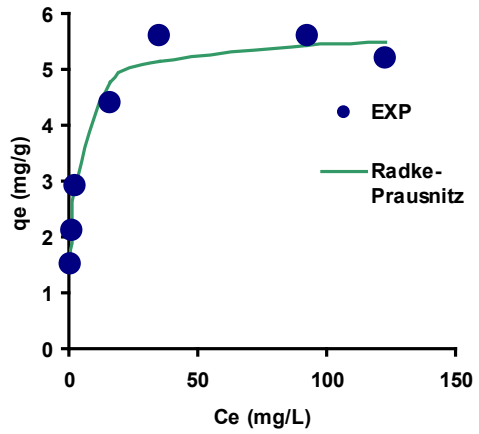

Fig. 14. Congo Red's adsorption isotherm onto kaolin as modelled using the Radke-Prausnitz isotherm model.

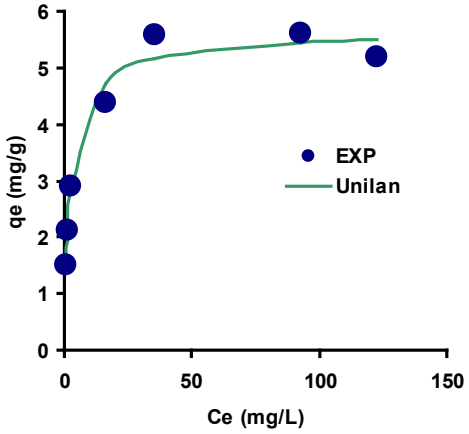

Fig. 17. Congo Red's adsorption isotherm onto kaolin as modelled using the Unilan isotherm model.

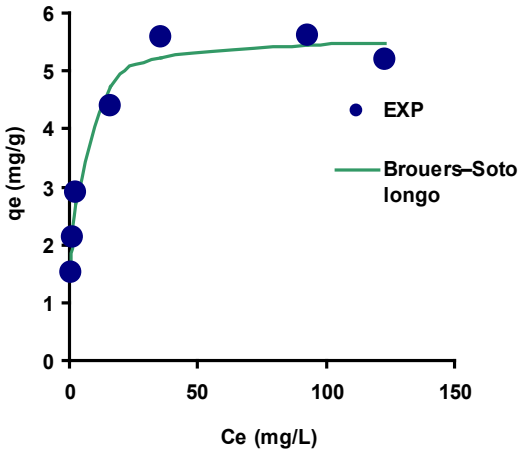

Fig. 15. Congo Red's adsorption isotherm onto kaolin as modelled using the Brouers-Sotolongo isotherm model.

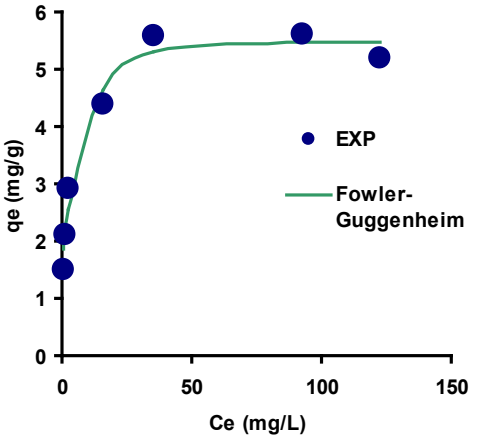

Fig. 18. Congo Red's adsorption isotherm onto kaolin as modelled using the Fowler Guggenheim isotherm model.

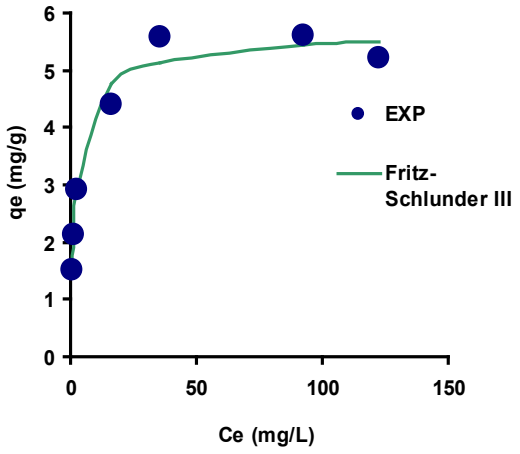

Fig. 16. Congo Red's adsorption isotherm onto kaolin as modelled using the Fritz-Schlunder III isotherm model.

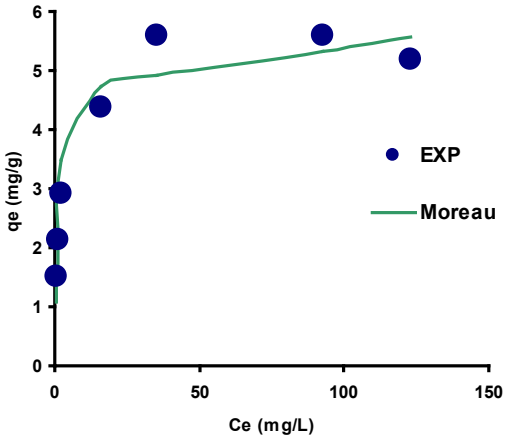

Fig. 19. Congo Red's adsorption isotherm onto kaolin as modelled using the Moreau isotherm model.

Table 2. Error function analysis for the fitting of the isotherm of Congo Red onto kaolin.

Model	No of parameter	RMSE	MPSD	adR^2	AICc	BIC	HQC	BF	AF
Henry	1	2.553	0.180	0.016	21.044	0.000	13.375	0.168	6.489
Langmuir	2	0.303	0.974	0.961	-1.091	13.990	-16.428	0.995	1.049
Freundlich	2	0.570	0.885	0.828	7.771	-15.199	-7.566	1.041	1.149
Temkin	3	0.338	0.974	0.948	14.909	-6.337	-15.096	0.995	1.049
Dubinin-Radushkevich	2	3.395	-70.72	-106.58	32.756	-13.253	17.419	0.165	6.538
Jovanovic	2	0.462	0.940	0.909	4.829	18.647	-10.508	0.983	1.089
Redlich-Peterson	3	0.309	0.978	0.956	13.622	-9.279	-16.384	1.000	1.044
Sips	3	0.296	0.979	0.959	13.058	-14.540	-16.948	1.003	1.052
Toth	3	0.310	0.978	0.955	13.675	-15.104	-16.330	1.000	1.044
Hill	3	0.296	0.979	0.959	13.058	-14.487	-16.948	1.003	1.052
Khan	3	0.311	0.978	0.955	13.735	-15.105	-16.270	0.999	1.044
BET	3	0.335	0.974	0.948	14.772	-14.427	-15.233	0.995	1.048
Vieth-Sladek	3	0.335	0.974	0.948	14.763	-13.390	-15.242	0.995	1.048
Radke-Prausnitz	3	0.311	0.978	0.955	13.735	-13.399	-16.271	0.999	1.044
Brouers–Sotolongo	3	0.293	0.980	0.960	12.907	-14.427	-17.098	1.006	1.064
Fritz-Schlunder III	3	0.309	0.978	0.956	13.622	-15.255	-16.384	1.000	1.044
Unilan	3	0.290	0.980	0.961	12.731	-14.540	-17.275	1.004	1.052
Fowler-Guggenheim	3	0.324	0.975	0.950	14.326	-15.431	-15.680	1.011	1.011
Moreau	3	0.542	0.936	0.871	21.507	-13.836	-8.499	0.964	0.964

Note:
RMSE Root mean Square Error
adR^2 Adjusted Coefficient of determination
p no of parameters
AF Accuracy factor
BF Bias factor
BIC Bayesian Information Criterion
AICc Adjusted Akaike Information Criterion
HQC Hannan–Quinn information criterion

Unilan (Unilin) model

Unilan is another empirical correlation mentioned in the book by Valenzuela and Myers which was suggested for the equilibrium data analysis. The name Unilin is also utilized in some publications where the term UniLan should be used instead. The term UniLan comes from "Uniform distribution and Langmuir local" isotherm. The Unilan equation assumes a patch-wise surface, with the local Langmuir equation valid on each patch [78].

In this isotherm, q_{mU} (mg g^{-1}) is the maximum monolayer adsorption capacity predicted by Unilan isotherm, a_U and b_U are the Unilan equilibrium constant and model exponent, respectively. b_U characterizes the heterogeneity of the system. The larger the value of this parameter, the system becomes more heterogeneous. If b_U =0, in this limit, the value for the range of energy distribution becomes zero, and the UniLan equation is converted to the classical Langmuir equation [79]. The result of the remodeling exercise, however, was not conform to the observed experimental q_m value of about 5 mg g^{-1} (**Table 3**).

Langmuir isotherm

Isotherm models typically span a spectrum from mechanistic to empirical, with the Langmuir isotherm falling firmly into the mechanistic category. This model postulates that adsorption occurs as a uniform monolayer on the adsorbent surface, assuming equal energy for all adsorption sites and structural homogeneity in the adsorbent [80]. Consequently, it predicts the formation of a monolayer coverage on the outer adsorbent surface due to the exponential decline in intermolecular interactions with increasing distance.

This simplifies the relationship into a linear form and posits a constant monolayer adsorption capacity. Moreover, it suggests that Henry's model is valid for both highly dilute and concentrated solute concentrations [81].

The Langmuir model, along with the Freundlich model, stands as one of the most commonly employed models in sorption studies. While the nonlinear regression approach yielded parameter predictions close to those in the original study, it was unable to provide a 95% confidence interval for the estimated parameters. The value of the maximum monolayer adsorption capacity for Congo Red binding to kaolin according to Langmuir's parameter q_{mL} was 5.49 mg g^{-1} (95% Confidence interval from 5.018 to 5.967), while b_L (L mg^{-1}), the Langmuir model constants was 0.5 L mg^{-1} (95% C.I. from 0.285 to 0.710). These values are very similar to the reported linear regressed values in the original publication for q_{mL} and b_L values at 5.44 mg g^{-1} and 0.50 L mg^{-1}, respectively [42]. The values obtained here are much lower than other adsorbents (**Table 4**).

Table 3. Isothermal models' constants for the top seven models.

Model		Unit	Value	(95% confidence interval)
Unilan	q_{mU}	mg g^{-1}	1.85	-4.913 to 8.610
	b_U		1.75	-1.552 to 5.053
	a_U		2.31	0.543 to 4.074
Brouers–Sotolongo	q_{mBS}	mg g^{-1}	5.48	4.791 to 6.172
	K_{BS}		0.43	0.274 to 0.593
	n_{BS}		1.82	0.932 to 2.706
Hill	q_{mH}	mg g^{-1}	5.701	4.561 to 6.842
	n_H		0.828	0.222 to 1.434
	K_H	L mg^{-1}	2.006	1.038 to 2.974
Sips	q_{mS}	mg g^{-1}	5.701	4.561 to 6.842
	K_S	L mg^{-1}	0.498	0.258 to 0.739
	n_S		1.21	0.323 to 2.092
Langmuir	q_{mL}	mg g^{-1}	5.49	5.018 to 5.967
	b_L	L mg^{-1}	0.50	0.285 to 0.710

Note
[#]Isotherms that have no direct way in estimating the maximum adsorption capacity (mg g^{-1}).

Table 4. Summary of Congo Red sorption by various adsorbents.

Adsorbent	Adsorption isotherm	q_m (mg g^{-1})	Reference
Cardamom peel	Langmuir	69.93 mg g^{-1}	[82]
Hydrogel Nanocomposite	Freundlich	-	[83]
Onion peel	Freundlich	91.53%	[84]
Amino-modified silica and graphene oxide	Langmuir	257.69 mg g^{-1}	[85]
Corn stalk derived cellulose		5572 mg g^{-1}	[86]
magnetic cellulose-based ionic liquid adsorbent	Langmuir	1299.3 mg g^{-1}	[87]
L-MOF-1 adsorbent	Langmuir	12000 mg g^{-1}	[88]
Ladder chain Cd-based polymer	Langmuir	16880 mg g^{-1}	[89]
Shrimp shell powder		276. 64 mg g^{-1}	[90]
Cellulose-based aerogel	Langmuir	518.40 mg g^{-1}	[91]
Crab shell	Langmuir	86.21 mg g^{-1}	[92]
Diethylenetriamine modified peanut shell cellulose	Langmuir	111.86 mg g^{-1}	[93]
Magnetic mesoporous titanium dioxide-graphene oxide (Fe3O 4@mTiO2@GO)	Freundlich	89.95 mg g^{-1}	[94]
Chitosan-coated quartz sand	Langmuir	96%	[95]
Groundnut shell carbon		-	[96]
Neem leaves	Langmuir	-	[97]

Brouers and Sotolongo

Brouers et al. [64] developed an isotherm model for adsorption on heterogeneous surfaces using a deformed exponential (Weibull) function, extending the classical Langmuir isotherm to account for non-uniform adsorbent surfaces. This model operates on the assumption that the adsorbent surface comprises multiple patches of active sites, each with identical energy levels. The application of empirical laws within previously established models like Freundlich, Redlich–Peterson, Toth, and Sips (Generalized Freundlich isotherms) is justified by the complex interplay of factors influencing adsorption, dependent on surface characteristics and pore structures.

The prevailing understanding is that lateral molecular interactions and surface heterogeneity, along with pore size distribution, offset each other's effects. This provides a rationale for the widespread adoption and successful use of these empirical formulations. In their study, Brouers et al. strive to establish a more physically grounded empirical set of isotherms, particularly through the exponent function, by considering a distribution of local isotherms that are averaged using a distribution of local adsorption energies, thereby advancing the foundation of adsorption modeling. Another way is to use a Monte Carlo simulation.

This model, which is very similar to the Jovanovic isotherm, presupposes that the pace at which the percentage of the surface that is not occupied by adsorbate molecules decreases is proportional to a specific power of the partial pressure of the adsorbate. This power is specified by the model [98]. In this model, the parameters appearing in the isotherm equation have a simple, clear physical interpretation. Thus, qm_{BS} is the maximum quantity biosorbed, K_{BS} measures how fast the sorption process progresses as C_e increases and the exponent $1/n_{BS}$, which is equal to or smaller than the Langmuir exponent ($1/n$), is a measure of the heterogeneity of the sorption energy distribution. The parameter n_{BS} is related with the distribution of adsorption energy and the energy of heterogeneity of the adsorbent surfaces at the given temperature.

Hill and Sips models

None of the isotherm models discussed thus far take into consideration the lateral interactions that can occur among adsorbate molecules on a solid surface. These interactions become notably stronger as the surface becomes more densely covered. In most scenarios, these intermolecular forces allow molecules attached to the solid surface to move relatively freely [99]. Consequently, these molecules must overcome potential barriers arising from the periodic structure of the solid surface and the subsequent periodic fluctuation in adsorption energy [100]. The Hill model was proposed, based on the concept of a mobile first layer adhering to a two-dimensional van der Waals' equation.

Nevertheless, the Hill model is most effective in situations with moderately high concentrations. It serves as an indicator of how strongly an adsorbent is attracted to the adsorbates it is designed to process due to the steepening effect it imparts on isotherm curves with increasing K_H. By adjusting the values of n_H, the Hill model can accurately describe a variety of isotherms, including S- and L-shaped curves. An S-shaped curve typically signifies attractive interactions among adsorbed species, but in this investigation, the n_H value is less than zero, suggesting the absence of a sigmoidal connection. Intriguingly, Chu et al. recently demonstrated that the Hill, Liu, Sips, and Koble–Corrigan isotherms are mathematically equivalent [101], a finding consistent with the identical maximum adsorption constants obtained for the Hill and Sips models in this study.

CONCLUSION

Nonlinear regression was applied to the adsorption isotherm data for Congo Red dye on kaolin, employing various models with one to three parameters each. Several evaluation metrics, including Root Mean Square Error (RMSE), adjusted coefficient of determination (adjR^2), bias factor (BF), accuracy factor (AF), bias information coefficient (BIC), and the corrected Akaike Information Criterion (AICc), consistently revealed that the Freundlich model outperformed the other models, emerging as the most suitable model based on comprehensive criteria assessment. The best isotherm model was found to be the Unilan followed by (descending order) Brouers–Sotolongo, Hill, Sips and Langmuir. The Unilan maximum adsorption capacity, shows a large deviation from the experimentally observed value with a large 95% confidence interval, indicating poor fitting parameters. The maximum adsorption capacity can be obtained using the next best models, which were Brouers–Sotolongo and Langmuir models. The fact that the value for the maximum adsorption constants of the Hill and Sips models are the same reiterates previous findings that both models are equivalent and only one of them should be used. The nonlinear regression approach represents parameter values in the 95% confidence interval range, which allows for better comparison with published findings.

REFERENCES

1. Haruna SD, Sufyan AJ, Ibrahim S, Babandi A, Shehu D, Ya'u M, et al. Characterization of Morganella sp. for its Paraquat Degradation Potential. Asian J Plant Biol. 2021 Dec 31;3(2):12–6.
2. Micky V, Nor Hasni H, Ennry E. Production of bioethanol from office waste via simultaneous saccharification fermentation. Bioremediation Sci Technol Res. 2014;2(1):19–22.
3. Uba G, Abdulhadi Y, Baiwa FI, Shehu Z, Abdulganiyyu IA. Analysis of Heavy Metals Levels in Locally produced Rice Fumigated with Cypermethrin (Pyrethroid) Pesticide Grown in Auyo Rice Field of Jigawa State. J Environ Bioremediation Toxicol. 2021 Jul 30;4(1):31–4.
4. Shettima H, Allamin IA, Halima N, Ismail HY, Musa Y. Isolation and Characterization of Hydrocarbon-degrading Bacteria in Soils of Mechanical Workshops in Maiduguri, Borno State. J Environ Bioremediation Toxicol. 2021 Dec 31;4(2):35–8.

5. Mohammed UY, Hamzah AP, Abubakar S. Consistent Organochlorinated Pesticides (OPC) Residues Contamination in Beans Consumed in Gombe Metropolis Nigeria. J Environ Bioremediation Toxicol. 2021 Dec 31;4(2):1–6.
6. Ghoniem E, Abdelgalil G, Gad A, Eshra ES. Molluscicidal Activity and Biochemical Interactions of Copper Sulfate against Theba pisana (Müller). Punjab Univ J Zool. 2022 Dec 5;37.
7. Sarker U, Ercisli S. Salt Eustress Induction in Red Amaranth (Amaranthus gangeticus) Augments Nutritional, Phenolic Acids and Antiradical Potential of Leaves. Antioxidants. 2022 Dec 9;11:2434.
8. Ghaju Shrestha R, Inoue D, IKE M. Effectiveness of Column-Type Two-Stage Constructed Wetlands for Simultaneous Removal of Organic Compounds and Heavy Metals Focusing on the Impact of Feeding Modes and Hydraulic Retention Time通水方式と流入負荷量に着目したカラム型二段人工湿地システムの有機物及び重金属類の同時除去に対する有効性の検討. Jpn J Water Treat Biol. 2022 Dec 15;58:137–48.
9. Tiimub B, Agyenta J, Azure A, Tiimob G, Osei-Bonsu R. Effectiveness of fluoride decontamination with Moringa oleifera and laterite from drinking water resources to safeguard public health at Bongo in Ghana. 2021 Mar 29;6:58–71.
10. Khan N, Islam MdS. State the organic pollution level in rain fed ponds, Noakhali, Bangladesh. 2019 Aug 5;438–41.
11. Khan N, Tisha N. Freshwater algal tolerance to organic pollution: a review. Pollut Res. 2020 Dec 1;39:1297–301.
12. Clayer F, Thrane JE, Ndungu K, King A, Dörsch P, Rohrlack T. Technical Note: Preventing CO 2 overestimation from mercuric or copper (II) chloride preservation of dissolved greenhouse gases in freshwater samples. 2023.
13. Hamad M. Comparing the performance of Cyperus papyrus and Typha domingensis for the removal of heavy metals, roxithromycin, levofloxacin and pathogenic bacteria from wastewater. Environ Sci Eur. 2023 Aug 7;35.
14. Md Yunus S, Hamzah Z, Ariffin NAN, Muslim MB. Cadmium, chromium, copper, lead, ferum and zinc levels in the cockles (Anadara granosa) from Kuala Selangor, Malaysia. Malays J Anal Sci. 2014;18(3):514–21.
15. Shinde R, Ingle P, Trivedi H, Wasule D, Gaharwar A, Gade A, et al. Bioremediation of industrial dye waste effluents aided by GIS applications: A comprehensive review. Environ Dev Sustain. 2023 Aug 16;
16. Matyszczak G, Jóźwik P, Zybert M, Yedzikhanau A, Krawczyk K. Dye-Modified, Sonochemically Obtained Nano-SnS 2 as an Efficient Photocatalyst for Metanil Yellow Removal. Materials. 2023 Aug 23;16:5774–1.
17. Philip I, Sarojini S, Biswas S, Jayaram S. Exploring the Potential of Bacillus velezensis, an Endophytic Bacteria Isolated from Alternanthera philoxeroides for Plant Growth Promotion and Bioremediation Properties. J Pure Appl Microbiol. 2023 Sep 2;17.
18. Zollinger H. Color Chemistry: Syntheses, Properties, and Applications of Organic Dyes and Pigments. John Wiley & Sons; 2003. 656 p.
19. Raghavendra KR, Ajay Kumar K. Synthesis of some novel azo dyes and their dyeing, redox and antifungal properties. Int J ChemTech Res. 2013;5(4):1756–60.
20. Patel B, Patel H. Current approaches toward the removal of methylene blue dye from synthetic textile effluent using bacterial treated agricultural waste absorbent through statistical design. Heliyon. 2023 Sep 1;9:e19857.
21. Kamble KD, More MA. Bacterial decolorization of acid yellow dye obtained from textile industry effluents. Int J Pharma Bio Sci. 2013;4(4):B763–9.
22. Methneni N, González JAM, Van Loco J, Anthonissen R, de Maele JV, Verschaeve L, et al. Ecotoxicity profile of heavily contaminated surface water of two rivers in Tunisia. Environ Toxicol Pharmacol. 2021 Feb 1;82:103550.
23. Sandhiya R, Begum KS, Charumathi D. Decolourization of triphenylmethane dyes and dye industry effluent by Staphylococcus aureus isolated from dye contaminated site. Int J Pharm Pharm Sci. 2016;8(9):258–66.
24. Kanhere J, Gopinathan R, Banerjee J. Cytotoxicity and genotoxicity of malachite green on non-target aquatic organisms: Chlorella pyrenoidosa and daphnia magna. Water Air Soil Pollut. 2014;225(9).
25. Przystas W, Zablocka-Godlewska E, Grabinska-Sota E. Biological removal of azo and triphenylmethane dyes and toxicity of process by-products. Water Air Soil Pollut. 2012;223(4):1581–92.
26. Konsowa AH. Decolorization of wastewater containing direct dye by ozonation in a batch bubble column reactor. Desalination. 2003;158(1–3):233–40.
27. Kishor R, Purchase D, Saratale GD, Saratale RG, Ferreira LFR, Bilal M, et al. Ecotoxicological and health concerns of persistent coloring pollutants of textile industry wastewater and treatment approaches for environmental safety. J Environ Chem Eng. 2021 Apr 1;9(2):105012.
28. Lellis B, Fávaro-Polonio CZ, Pamphile JA, Polonio JC. Effects of textile dyes on health and the environment and bioremediation potential of living organisms. Biotechnol Res Innov. 2019 Jul 1;3(2):275–90.
29. Dogan EE, Yesilada E, Ozata L, Yologlu S. Genotoxicity testing of four textile dyes in two crosses of drosophila using wing somatic mutation and recombination test. Drug Chem Toxicol. 2005;28(3):289–301.
30. Yusuf F, Yakasai HM, Usman S, Muhammad JB, Yaú M, Jagaba AH, et al. Dyes-decolorizing potential of fungi strain BUK_BCH_BTE1 locally isolated from textile industry effluents: Characterization and LC-MS analysis of the metabolites. Case Stud Chem Environ Eng. 2023 Dec 1;8:100453.
31. Karaman C, Karaman O, Show PL, Karimi-Maleh H, Zare N. Congo red dye removal from aqueous environment by cationic surfactant modified-biomass derived carbon: Equilibrium, kinetic, and thermodynamic modeling, and forecasting via artificial neural network approach. Chemosphere. 2022 Mar 1;290:133346.
32. Igwegbe CA, Ighalo JO, Onyechi KK, Onukwuli OD. Adsorption of Congo red and malachite green using H3PO4 and NaCl-modified activated carbon from rubber (Hevea brasiliensis) seed shells. Sustain Water Resour Manag. 2021 Jul 28;7(4):63.
33. Ghanavati Nasab S, Semnani A, Teimouri A, Kahkesh H, Momeni Isfahani T, Habibollahi S. Removal of Congo Red from Aqueous Solution by Hydroxyapatite Nanoparticles Loaded on Zein as an Efficient and Green Adsorbent: Response Surface Methodology and Artificial Neural Network-Genetic Algorithm. J Polym Environ. 2018;26(9):3677–97.
34. Xiang P, Zhang T, Wu Q, Li Q. Systematic Review of Degradation Processes for Microplastics: Progress and Prospects. Sustainability. 2023 Aug 22;15:12698.
35. Chandran D, Muruganandam L, Biswas R. A review on adsorption of heavy metals from wastewater using carbon nanotube and graphene-based nanomaterials. Environ Sci Pollut Res. 2023 Oct 7;
36. Amri A, Rezonsi R, Ahmad N, Taher T, Palapa N, Mohadi R, et al. Biochar-Modified Layered Double Hydroxide for Highly Efficient on Phenol Adsorption. Bull Chem React Eng Catal. 2023 Sep 21;18:460–72.
37. Lian J, Zhou F, Chen B, Yang M, Wang S, Liu Z, et al. Enhanced adsorption of molybdenum(VI) onto drinking water treatment residues modified by thermal treatment and acid activation. J Clean Prod [Internet]. 2020;244. Available from: https://www.scopus.com/inward/record.uri?eid=2-s2.0-85073111312&doi=10.1016%2fj.jclepro.2019.118719&partnerID=40&md5=0e2c7b75605e08137bf6cf5f98e16cea
38. Chattrairat K, Phromyothin D. Synthesis of kaolinite/magnetic molecularly imprinted polymers for solid phase extraction of chlorpyrifos. Jpn J Appl Phys. 2019;58(SD).
39. Kamal S, Kamal A, Shahzad T, Rehman S, Azeem M, Bibi I. Potential of kaolinite as adsorbent to remove anionic surfactant from simulated industrial wastewater. Desalination Water Treat. 2017;88:85–92.
40. Tehrani-Bagha AR, Nikkar H, Mahmoodi NM, Markazi M, Menger FM. The sorption of cationic dyes onto kaolin: Kinetic, isotherm and thermodynamic studies. Desalination. 2011;266(1–3):274–80.
41. Motulsky HJ, Ransnas LA. Fitting curves to data using nonlinear regression: a practical and nonmathematical review. FASEB J. 1987;1(5):365–74.
42. Vimonses V, Lei S, Jin B, Chow CWK, Saint C. Kinetic study and equilibrium isotherm analysis of Congo Red adsorption by clay materials. Chem Eng J. 2009 May 15;148(2):354–64.
43. Tawfik GM, Dila KAS, Mohamed MYF, Tam DNH, Kien ND, Ahmed AM, et al. A step by step guide for conducting a systematic

review and meta-analysis with simulation data. Trop Med Health. 2019 Aug 1;47(1):46.
44. Khare KS, Phelan FR. Quantitative Comparison of Atomistic Simulations with Experiment for a Cross-Linked Epoxy: A Specific Volume-Cooling Rate Analysis. Macromolecules. 2018;51(2):564–75.
45. Langmuir I. THE ADSORPTION OF GASES ON PLANE SURFACES OF GLASS, MICA AND PLATINUM. J Am Chem Soc. 1918;40(2):1361–402.
46. Schirmer W. Physical Chemistry of Surfaces. Z Für Phys Chem. 1999;210(1):134–5.
47. Ridha FN, Webley PA. Anomalous Henry's law behavior of nitrogen and carbon dioxide adsorption on alkali-exchanged chabazite zeolites. Sep Purif Technol. 2009;67(3):336–43.
48. Jovanović DS. Physical adsorption of gases - I: Isotherms for monolayer and multilayer adsorption. Kolloid-Z Amp Z Für Polym. 1969;235(1):1203–13.
49. Carmo AM, Hundal LS, Thompson ML. Sorption of hydrophobic organic compounds by soil materials: Application of unit equivalent Freundlich coefficients. Environ Sci Technol. 2000;34(20):4363–9.
50. Radushkevich LV. Potential theory of sorption and structure of carbons. Zhurnal Fiz Khimii. 1949;23:1410–20.
51. Dubinin MM. Modern state of the theory of volume filling of micropore adsorbents during adsorption of gases and steams on carbon adsorbents. Zh Fiz Khim. 1965;39(6):1305–17.
52. Temkin MI, Pyzhev V. Kinetics of ammonia synthesis on promoted iron catalysts. Acta Physicochim USSR. 1940;12(3):327–56.
53. Chu KH. Revisiting the Temkin Isotherm: Dimensional Inconsistency and Approximate Forms. Ind Eng Chem Res [Internet]. 2021 Aug 16 [cited 2022 Sep 1]; Available from: https://pubs.acs.org/doi/pdf/10.1021/acs.iecr.1c01788
54. Redlich O, Peterson DL. A Useful Adsorption Isotherm. Shell Dev Co Emeryv Calif. 1958;63:1024.
55. Sips R. On the structure of a catalyst surface. J Chem Phys. 1948;16(5):490–5.
56. Tóth J. Uniform interpretation of gas/solid adsorption. Adv Colloid Interface Sci. 1995;55(C):1–239.
57. Hill AV. The possible effects of the aggregation of the molecules of haemoglobin on its dissociation curves. J Physiol. 1910;40:iv–vii.
58. Khan AA, Singh RP. Adsorption thermodynamics of carbofuran on Sn (IV) arsenosilicate in H+, Na+ and Ca2+ forms. Colloids Surf. 1987;24(1):33–42.
59. Brunauer S, Emmett PH, Teller E. Adsorption of Gases in Multimolecular Layers. J Am Chem Soc. 1938;60(2):309–19.
60. Vieth WR, Sladek KJ. A model for diffusion in a glassy polymer. J Colloid Sci. 1965;20(9):1014–33.
61. Radke CJ, Prausnitz JM. Adsorption of Organic Solutes from Dilute Aqueous Solution of Activated Carbon. J Am Chem Soc. 1972;11(4):445–51.
62. Liu Y, Liu YJ. Biosorption isotherms, kinetics and thermodynamics. Sep Purif Technol. 2008;61(3):229–42.
63. Tran HN, Bollinger JC, Lima EC, Juang RS. How to avoid mistakes in treating adsorption isotherm data (liquid and solid phases): Some comments about correctly using Radke-Prausnitz nonlinear model and Langmuir equilibrium constant. J Environ Manage. 2023 Jan 1;325(Pt A):116475.
64. Brouers F, Sotolongo O, Marquez F, Pirard JP. Microporous and heterogeneous surface adsorption isotherms arising from Levy distributions. Phys Stat Mech Its Appl. 2005 Apr 1;349(1):271–82.
65. Hamissa AMB, Brouers F, Mahjoub B, Seffen M. Adsorption of Textile Dyes Using Agave Americana (L.) Fibres: Equilibrium and Kinetics Modelling. Adsorpt Sci Technol. 2007 Jun 1;25(5):311–25.
66. Fritz W, Schluender EU. Simultaneous adsorption equilibria of organic solutes in dilute aqueous solutions on activated carbon. Chem Eng Sci. 1974;29(5):1279–82.
67. Chu KH, Tan B. Is the Frumkin (Fowler–Guggenheim) adsorption isotherm a two- or three-parameter equation? Colloid Interface Sci Commun. 2021 Nov 1;45:100519.
68. Martucci A, Braschi I, Bisio C, Sarti E, Rodeghero E, Bagatin R, et al. Influence of water on the retention of methyl tertiary-butyl ether by high silica ZSM-5 and Y zeolites: A multidisciplinary study on the adsorption from liquid and gas phase. RSC Adv. 2015;5(106):86997–7006.
69. Baudu M. Etude des interactions solute–fibres de charbon actif. Application et regeneration. Universite de Rennes I; 1990.
70. Parker Jr. GR. Optimum isotherm equation and thermodynamic interpretation for aqueous 1,1,2-trichloroethene adsorption isotherms on three adsorbents. Adsorption. 1995;1(2):113–32.
71. van Vliet BM, Weber Jr WJ, Hozumi H. Modeling and prediction of specific compound adsorption by activated carbon and synthetic adsorbents. Water Res. 1980;14(12):1719–28.
72. Burnham KP, Anderson DR. Multimodel inference: Understanding AIC and BIC in model selection. Sociol Methods Res. 2004;33(2):261–304.
73. Akaike H. A New Look at the Statistical Model Identification. IEEE Trans Autom Control. 1974;19(6):716–23.
74. Dan-Iya BI, Shukor MY. Isothermal Modelling of the Adsorption of Chromium onto Calcium Alginate Nanoparticles. J Environ Microbiol Toxicol. 2021;9(2):1–7.
75. Marquardt DW. An Algorithm for Least-Squares Estimation of Nonlinear Parameters. J Soc Ind Appl Math. 1963;11(2):431–41.
76. Seidel A, Gelbin D. On applying the ideal adsorbed solution theory to multicomponent adsorption equilibria of dissolved organic components on activated carbon. Chem Eng Sci. 1988 Jan 1;43(1):79–88.
77. Porter JF, McKay G, Choy KH. The prediction of sorption from a binary mixture of acidic dyes using single- and mixed-isotherm variants of the ideal adsorbed solute theory. Chem Eng Sci. 1999;54(24):5863–85.
78. Valenzuela DP, Myers AL. Adsorption equilibrium data handbook. Englewood Cliffs, N.J: Prentice Hall; 1989. 366 p.
79. McKay G, Mesdaghinia A, Nasseri S, Hadi M, Solaimany Aminabad M. Optimum isotherms of dyes sorption by activated carbon: Fractional theoretical capacity & error analysis. Chem Eng J. 2014;251:236–47.
80. Langmuir I. The constitution and fundamental properties of solids and liquids. Part I. Solids. J Am Chem Soc. 1916;38(11):2221–95.
81. Foo KY, Hameed BH. Insights into the modeling of adsorption isotherm systems. Chem Eng J. 2010;156(1):2–10.
82. Ahmad Aftab R, Zaidi S, Aslam Parwaz Khan A, Arish Usman M, Khan AY, Tariq Saeed Chani M, et al. Removal of congo red from water by adsorption onto activated carbon derived from waste black cardamom peels and machine learning modeling. Vol. 71, Alexandria Engineering Journal. 2023. p. 355–69.
83. Alhattab ZD, Aljeboree AM. Modification, Preparation, and Characterization, Low-Cost Hydrogel Nano/Micro Composite: Regeneration and Isotherm Models. Vol. 6, Journal of Medicinal and Chemical Sciences. 2023. p. 152–9.
84. Salimi Shahraki H, Qurtulen, Ahmad A. Synthesis, characterization of carbon dots from onion peel and their application as absorbent and anticancer activity [Internet]. Vol. 150, Inorganic Chemistry Communications. 2023. Available from: https://www.scopus.com/inward/record.uri?eid=2-s2.0-85148677144&doi=10.1016%2fj.inoche.2023.110514&partnerID=40&md5=d55cfc7aa849165ec672df748b402527
85. Cheng L, Zhang L, Wang H, Song F. Simultaneous removal of Congo red and Cr(VI) using amino-modified GO/MS composite materials. Vol. 39, Korean Journal of Chemical Engineering. 2022. p. 1257–67.
86. Wang R, Liu Y, Lu Y, Liang S, Zhang Y, Zhang J, et al. Fabrication of a corn stalk derived cellulose-based bio-adsorbent to remove Congo red from wastewater: Investigation on its ultra-high adsorption performance and mechanism [Internet]. Vol. 241, International Journal of Biological Macromolecules. 2023. Available from: https://www.scopus.com/inward/record.uri?eid=2-s2.0-85153510968&doi=10.1016%2fj.ijbiomac.2023.124545&partnerID=40&md5=6afbefa4ef22b4ad65c577b9544fca8c
87. Ling C, Yimin D, Qi L, Chengqian F, Zhiheng W, Yaqi L, et al. Novel High-efficiency adsorbent consisting of magnetic Cellulose-based ionic liquid for removal of anionic dyes [Internet]. Vol. 353, Journal of Molecular Liquids. 2022. Available from: https://www.scopus.com/inward/record.uri?eid=2-s2.0-85125627705&doi=10.1016%2fj.molliq.2022.118723&partnerID=40&md5=99302ae978cd5e1dd45d08d5c7aab205
88. Guo DD, Li B, Deng ZP, Huo LH, Gao S. A rational design of layered metal-organic framework towards high-performance

adsorption of hazardous organic dye. Vol. 50, Dalton Transactions. 2021. p. 7818–25.
89. Guo DD, Li B, Deng ZP, Huo LH, Gao S. Ladder chain Cd-based polymer as a highly effective adsorbent for removal of Congo red. Vol. 178, Ecotoxicology and Environmental Safety. 2019. p. 221–9.
90. Wu Q, Dai L, Yang W, Ge L, Xia M. Adsorption of cationic and anionic dyes from aqueous solutions by shrimp shell powder; [虾壳粉对水溶液中阴、阳离子型染料的吸附]. Vol. 13, Chinese Journal of Environmental Engineering. 2019. p. 594–606.
91. Wang Y, Zhao L, Hou J, Peng H, Wu J, Liu Z, et al. Kinetic, isotherm, and thermodynamic studies of the adsorption of dyes from aqueous solution by cellulose-based adsorbents. Vol. 77, Water Science and Technology. 2018. p. 2699–708.
92. Dai L, Yao Z, Yang W, Xia M, Ye Y. Crab shell: A potential high-efficiency and low-cost adsorbent for dye wastewater. Vol. 26, Fresenius Environmental Bulletin. 2017. p. 4991–8.
93. Tang J, Fan K. Adsorption of Congo red from aqueous solutions by diethylenetriamine modified peanut shell cellulose. Vol. 10, Chinese Journal of Environmental Engineering. 2016. p. 4201–5.
94. Li L, Li X, Duan H, Wang X, Luo C. Removal of Congo Red by magnetic mesoporous titanium dioxide-graphene oxide core-shell microspheres for water purification. Vol. 43, Dalton Transactions. 2014. p. 8431–8.
95. Feng T, Zhang F, Wang J, Wang L. Application of chitosan-coated quartz sand for Congo red adsorption from aqueous solution. Vol. 125, Journal of Applied Polymer Science. 2012. p. 1766–72.
96. Kannan N, Meenakshisundaram M. Studies on the removal of dyes by adsorption onto groundnut shell carbon. Vol. 29, Indian Journal of Environmental Protection. 2009. p. 902–7.
97. Raghuvanshi SP, Singh R, Kaushik CP. Adsorption of congo red dye from aqueous solutions using neem leaves as adsorbent. Vol. 20, Asian Journal of Chemistry. 2008. p. 4994–5000.
98. Brouers F, Marquez-Montesino F. Dubinin isotherms versus the Brouers-Sotolongo family isotherms: A case study. Adsorpt Sci Technol. 2016 Oct 10;34.
99. Witkiewicz Z, Grajek H, Neffe S. Chromatographic determination of the physico-chemical parameters of adsorption on active carbons. J Chromatogr A. 1991 Jan 1;556:441–56.
100. Hill TL. Statistical mechanics of multimolecular adsorption ii. localized and mobile adsorption and absorption. J Chem Phys. 2004 Dec 22;14(7):441–53.
101. Chu KH, Debord J, Harel M, Bollinger JC. Mirror, Mirror on the Wall, Which Is the Fairest of Them All? Comparing the Hill, Sips, Koble–Corrigan, and Liu Adsorption Isotherms. Ind Eng Chem Res. 2022 May 18;61(19):6781–90.